# Wnt Signalling Controls the Response to Mechanical Loading during Zebrafish Joint Development

**Authors:** L H Brunt, K Begg, E Kague, S Cross, C L Hammond

Lucy H Brunt
Physiology, Pharmacology and Neuroscience,
University of Bristol
Bristol, UK

Katie Begg
Physiology, Pharmacology and Neuroscience
University of Bristol
Bristol, UK

Erika Kague
Physiology, Pharmacology and Neuroscience
University of Bristol
Bristol, UK

Stephen Cross
Wolfson Bioimaging Facility,
University of Bristol
Bristol, UK

Chrissy L Hammond
Physiology, Pharmacology and Neuroscience
University of Bristol
Bristol, UK

**Corresponding author:**

Chrissy L Hammond
Chrissy.hammond@bristol.ac.uk

***Abstract***

Normal joint morphogenesis requires mechanical activity during development. Loss of mechanical strain causes abnormal joint development, which can impact long term joint health. While proliferation and changes to cell orientation are known to shape the joint, dynamic imaging of a developing joint *in vivo* has not been possible in other species. Using genetic labelling techniques in zebrafish such as photo-conversion of kaede and multi-spectral Zebrabow transgenic lines we were able, for the first time, to dynamically track cell behaviours in intact moving joints of individually labelled larvae. We identify that joint cell proliferation and migration, which contribute to normal joint morphogenesis, are mechanically controlled and are significantly reduced in immobilised larvae. By comparison to strain maps of the developing skeleton we identify canonical Wnt signalling as a candidate to transduce the mechanical forces into cell behaviours in the developing joint. We show that in the jaw Wnt signalling is reduced specifically in regions of high strain such as the interzone and developing ligaments, in response to loss of muscle activity through immobilisation. By pharmacological manipulation of canonical Wnt signalling we demonstrate that Wnt acts downstream of mechanical activity and is required for correct joint patterning and chondrocyte maturation. Knockdown of Wnt16 alone, leads to loss of Wnt response specifically in joint associated tissues. Finally, we demonstrate that Wnt16, independent of muscle activity, controls joint cell proliferation and migration, but plays no role in chondrocyte intercalation.

***Introduction***

The developing skeleton is subject to many biomechanical forces, including those from fetal/early postnatal muscle activity. It has become increasingly clear from studies on animal models that mechanical stimuli are required for accurate and functional joint formation [Reviewed in 1, 2]. For example, *Pax3*$^{sp/sp}$ (*splotch)* mutant mice, that lack limb muscle and *Myf5* $^{-/-}$*MyoD*$^{-/-}$ double mutants that lack all muscle, show altered morphology in many different joints including elbow and shoulder joints [3-7]. In chick, paralysis or removal of muscle through grafts results in a knee joint that lacks

refinement [8, 9]. Zebrafish mutants that lack neuromuscular nicotinic receptors (*nic* b107) and are therefore immobile, display jaw morphology abnormalities, such as smaller and wider elements [10]. Zebrafish jaw joint morphology is also affected by paralysis, particularly in regions associated with high compressive strain [11, 12]. In humans, biomechanical stimuli *in utero* and in newborns has been found to have a long-term impact on skeletal health [Reviewed in 13]. For example, Foetal Akinesia Deformation Sequence, (FADS), can cause arthrogryposis due to reduced foetal movement [14]. Risk factors such as breech birth [15] and swaddling that restrict hip joint movement [16] can also cause hip joint abnormalities in the condition Developmental Dysplasia of the hip (DDH), [17]. If left untreated, the abnormal joint shape in DDH can lead to early onset osteoarthritis (OA) [18]. Thus, diverse vertebrate species ranging from fish to humans rely on muscle activity to provide a mechanical stimulus to activate the cellular processes required to shape joints during development. This process also has an impact on joint function and health later in life.

Mechanical stimulus can activate genes important for skeletogenesis. *In vitro* experiments have shown that application of force to chondrocytes can lead to activation of genes, including those encoding cartilage matrix proteins; such as Type II collagen and Aggrecan and proteins involved in GAG synthesis [Reviewed in 19]. Biomechanical stimuli have been widely documented to regulate signalling genes involved in bone formation in vivo including constituents of the BMP pathway and *Ihh* [Reviewed in 20, 21]. For mechanical activity to shape the skeleton, alterations to cell behaviour need to occur. A reduction in cell proliferation has been reported in regions of the joint affected morphologically by immobilisation, such as the intercondylar fossa in chick knee joints, mouse mandibular condyles and the joint interzone of *splotch* mice [3, 22, 23]. Cell orientation changes are also seen in cartilage elements and at jaw joints in zebrafish models that lack muscle activity [10, 11]. Mechanical stimuli are also required for tendon and ligament formation and maturation in species ranging from zebrafish to humans [24, reviewed in 25]. Although cell proliferation and orientation at joints have been shown to be biomechanically controlled, as yet, the signals and

pathways that transduce the mechanical stimuli into a cellular response have not been fully elucidated.

Wnts are a family of secreted signalling glycoprotein molecules that play vital roles in development, health and disease [Reviewed in 26]. Classically, Wnt ligands were subdivided into those that activate the canonical beta-catenin pathway or that activate the non-canonical pathways such as Planar Cell polarity (PCP) and calcium-mediated pathways. However, a more recent consensus is that control of the pathway is interlinked and that Wnt ligands can activate multiple pathways depending on the tissue type and cellular context [Reviewed in 27]. Many Wnts including Wnt4, Wnt5b and Wnt9a; which typically operate in the canonical pathway, and non-canonical Wnt5a are expressed in developing skeletal elements and are implicated in roles such as regulation of chondrocyte differentiation [28-30] and joint cell identity [31, 32]. Wnt4, Wnt16, Wnt11 and sFRP2 are all expressed at developing joints [31, 33-36]. Members of the Wnt signalling pathway have also been identified as mechanosensitive. For example, dynamic loading of cultured mesenchymal stem cells affects the regulation of Wnt related genes such as Frizzled-7, Wnt3, Wnt5a and Wnt8 [37, 38]. A decrease in canonical beta-catenin activation was found in 'muscleless' *Pax3*$^{sp/sp}$ *Splotch* mouse mutants at the joint site [3]. A transcriptomic study comparing changes to gene expression in humerus tissue between control and Pax3$^{sp/sp}$ *Splotch* mouse mutants demonstrated that loss of limb muscle led to dysregulation of 34 members of the Wnt signalling pathway; more genes than any other signalling pathway [35]. These included Wnt ligands, Wnt modulators, such as Srfp2 and downstream targets, such as CD44. Therefore, Wnt signalling activity in skeletal tissue is mechanosensitive and a candidate pathway to act downstream of mechanical stimuli in skeletogenesis. However, it is unknown whether Wnt signalling is required for the cellular changes occurring during skeletogenesis and joint morphogenesis.

Here, we describe cell behaviours that contribute to changes in joint morphology by following live zebrafish joint development under normal or reduced biomechanical conditions. We demonstrate

that canonical Wnt activity transduces mechanical signalling to bring about cell behaviours such as proliferation, migration, intercalation and cell morphology changes required to shape the joint. We show that Wnt16 controls cell proliferation and migration specifically in cells at the jaw joint of the lower jaw.

## *Methods*

### Zebrafish husbandry and transgenic lines

Zebrafish were maintained as previously described [39]. Experiments were approved by the local ethics committee and were granted a UK Home Office project licence. Transgenic lines *Tg(7xTCF.XlaSiam:nlsGFP)* [40], *Tg(Col2a1aBAC:mcherry)* [41], *Tg(Sox10:GAL4-VP16)* [42], *Tg(UAS:Kaede)* [43], *Tg(ubi:Zebrabow)* [44] and *Tg( -4.7Sox10:cre)* [45] have been previously described.

### Pharmacological treatment

Fish were anaesthetised between 3 and 5 days post fertilisation (dpf) with 0.1mg/ml MS222 (Tricaine methanesulfonate) (Sigma) diluted in Danieau solution. MS222 and Danieau solution was refreshed twice daily. 20µM IWR-1 (Sigma); which stabilises Axin in the beta-catenin destruction complex, was diluted in Danieau solution and replaced daily.

### Finite Element (FE) models

Meshes for the 5dpf FE models have been previously described and published [11, 46]. Loads for jaw opening (Protractor Hyoideus and Intermandibularis Anterior muscles) and jaw closure (Adductor Mandibulae muscles) were applied to predict tensile and compressive strains. FE results are displayed as colour coded contour plots of maximum and minimum strain.

### Wnt responsive cell counts and area

Image stacks of 4 and 5dpf *Tg(7xTCF.XlaSiam:nlsGFP) xTg(Col2a1aBAC:mcherry)* transgenic jaws were imported into Fiji [47]. Wnt responsive cells of ligament and tendon morphology along the palatoquadrate (PQ) element were counted. All Wnt responsive cells surrounding the jaw joint within a 50x80 µm area were counted.

A custom script was written in MATLAB (version 2015a; Mathworks, Inc.) so that a selected area of *Tg(7xTCF.XlaSiam:nlsGFP)* GFP positive signal could be determined. Areas of interest included: 1. the area of the Meckel's Cartilage (MC) (from 6 intercalating cells above the MC joint) plus the PQ, 2. the joint region (from 6 intercalating cells above the MC joint, to the MC interzone). Coarse regions of interest were initially manually identified from maximum intensity projections of the image stack and subsequently segmented in 3 dimensions (3D) based on the MATLAB implementation of Otsu's threshold [48]. All voxels within a user-selected region of interest with intensity values above the threshold were classified as a single object. An alpha shape was calculated for each segmented object [49] using MATLAB's automatically determined surface radius. Volumes for each object were measured using the method provided by the MATLAB alpha shape class.

**Wholemount Immunohistochemistry**

Larvae were fixed in 4% paraformaldehyde (PFA) for 1 hour (hr) at room temperature (RT) and dehydrated for storage in 100% MeOH until required. Larvae were rehydrated into phosphate buffered saline with 0.1% Tween-20 (PBT) in 3x 5 minute washes, permeabilised using 0.25% trypsin on ice for 7 minutes (for anti-myosin) or with 15µg/ml Proteinase K at 37°C (for anti- tenascin C & anti-BrdU) and washed 3x 5 minutes (mins) in PBT. Larvae were refixed in 4% PFA for 20mins at RT and washed 3x5mins in PBT. Larvae to be immunostained for BrdU were treated with 2N HCl for 1hr at 37°C and then extensively washed with PBT. All larvae were blocked in 5% Horse serum (HS) in PBT for 2-3 hours. Larvae were incubated in 5% HS in PBT blocking buffer with the appropriate dilution of antibodies overnight at 4°C (Chicken anti-GFP, Abcam, 1:500 dilution; mouse anti-myosin A4.1025, Developmental Studies Hybridoma Bank (DSHB), 1:500 dilution; rabbit anti-tenascin C, US

biological, 1:300 dilution; mouse anti-BrdU, Sigma, 1:100 dilution; rabbit anti-collagen II, abcam, 1:200 dilution). Larvae were washed in PBT 6x15 mins, before blocking in 5% HS in PBT for 1-2 hrs, then incubated overnight at 4°C in secondary antibody (Dylite 550 goat anti-mouse IgG, Dylite 488 goat anti-mouse IgG, Dylite 550 goat anti-rabbit IgG, Dylite 488 goat anti-chicken, IgY, Molecular Probes, 1:500 dilution), before washing 6x 15 mins in PBT prior to imaging on confocal SP8.

**Joint outline and interzone interval analysis**

Tiff images of *Tg(Col2a1aBAC:mcherry)* transgenic labelled joints were imported into Powerpoint. The draw tool was used to draw around 4 representative joints for each condition and overlaid for analysis.

The interval between the MC and PQ cartilage elements on the medial and lateral side of the jaw joint were measured from tiff images in LAS AF Lite software. Negative values correspond to instances of overlapping cartilage elements.

**Kaede protein photoconversion**

Double transgenic *Tg(Sox10:GAL4-VP16) x Tg(UAS:Kaede)* zebrafish larvae at 3dpf were mounted ventrally on coverslips in 0.3% agarose under MS222 anaesthetic. The FRAP wizard setting on the Leica LAS software was used to photoconvert kaede expressing cells of interest from green to red fluorescence on a Leica SP5 or SP8 microscope. Briefly, a region of interest (ROI) was drawn using the selection tools, on the medial region of the Meckel's cartilage joint or on the intercalating cell region of the MC. The 405nm was used to photoconvert kaede protein expressing cells in the ROI with settings of 8% laser power for 10 seconds. Following photoconversion, larvae were removed from agarose and flushed with fresh Danieau solution until resumption of movement. Each larva was kept separately for individual identification. Larvae were then left to develop normally or anaesthetised with MS222 and reimaged at 5dpf. Daughter cells inherit irreversibly photoconverted red kaede protein after cell division [50].

178 **Photoconverted cell number and area change**

179 Image stacks containing the red channel were imported into Fiji software [47] and red kaede
180 expressing cell numbers were counted at 3 and 5 dpf. The percentage increase in cell number was
181 then calculated.

182 The image stacks were saved as a tiff file. A Fiji plugin designed to segment out a thresholded level of
183 red cells was used to calculate the combined area of red cells. The combined area of cells expressing
184 red kaede protein was compared from the individual larvae from 3 to 5 dpf. The percentage increase
185 in cell area was then calculated.

186 **Jaw and element length and ratio of cell type in MC element**

187 Confocal images of the jaw joint region labelled with Tg(Col2a1aBAC:mcherry) were loaded into Fiji
188 [47]. The length (µm) of the jaw was measured from the anterior MC to the posterior
189 palatoquadrate using the line tool. The length of the MC element was measured using the freehand
190 line tool from the anterior MC to the MC jaw joint. The proportion of the length (µm) of the MC
191 taken up by rounded cells at the jaw joint or by intercalating cells was measured in Fiji using the
192 freehand line tool. The ratio of the length of the MC occupied by varying cell types compared to the
193 full MC length was then calculated.

194 **BrdU**

195 Larvae were treated with 3mM BrdU (Sigma) diluted in Danieau solution from 3-4dpf or 4-5dpf. After
196 treatment, larvae were washed 4x5min in Danieau solution then fixed with 4% PFA overnight at 4°C.
197 Larvae were then immunostained for BrdU (as detailed above).

198 **Zebrabow**

199 Double transgenic (*Tg(Ubi:Zebrabow)*) and *Tg(Sox10:Cre)* zebrafish larvae express a wide variety of
200 different fluorescent protein combinations in the cells of the developing cartilage. This allows

individual cells to be tracked as they migrate or divide. 3dpf *Tg(Sox10:Cre)* x *Tg(Ubi:Zebrabow)* double transgenic zebrafish were mounted in 0.3% agarose on coverslips in dishes and covered with Danieau solution containing MS222. The larvae were imaged on a Leica Multiphoton microscope using a 25x water dipping lens. Three fluorescence channels were collected individually (YFP, RFP and GFP). Larvae were returned to fresh Danieau solution in individual dishes and either left to develop normally or anaesthetised with MS222 until 5dpf, then reimaged.

**Wnt16 Morpholino knockdown**

A Wnt16 splice-blocking morpholino (MO) (Gene-Tools), AGGTTAGTTCTGTCACCCACCTGTC was used to knockdown Wnt16 protein as previously described [51]. 5ng of Wnt16 or control morpholino was injected with rhodamine dextran and 0.2M potassium chloride into 1 cell stage *Tg(Sox10:GAL4-VP16) x Tg(UAS:Kaede)* embryos using a picospritzer III (Parker) microinjector.

**RNA extraction and making Wnt16 cDNA**

Failure of splicing after Wnt16 MO injection was confirmed by PCR (S1A Fig). Total RNA was extracted from pooled and homogenised 3dpf Wnt16 MO injected and control non-injected larvae using a Nucleospin RNA II kit, (Macherey-Nagel). cDNA was produced from 1µg RNA via reverse transcription using M-MLV reverse transcriptase (Promega). cDNA was amplified by PCR using Wnt16 primers (forward: ACTAAAGAGACAGCTTCATCC, reverse: AACTCATCTTTGGTGATAGGC, (Eurofins Genomics)) [51] and Taq polymerase (Roche). PCR conditions are previously described [51].

**Mouth movements**

Zebrafish anaesthetised with MS222 were mounted laterally on coverslips in 1% agarose. Forceps were used to remove the agarose from around the head and fresh Danieau solution was repeatedly flushed over the agarose-free cavity around the head until normal jaw movements resumed. The number of jaw movements in 1 minute were recorded, using a stereo microscope.

### In situ hybridisation

*In situ hybridisation* was performed as previously described [52], using a probe for *lef1* on 3dpf larvae. *Lef1* plasmid in a pBS-SK vector with Ampicillin resistance was delinearised using EcoRI and transcribed using T7. Samples were stored in 70% glycerol and whole mount larvae were then imaged using a stereo microscope or the jaws were dissected out onto slides and imaged using a compound microscope.

### Statistics

Statistics were performed using SPSS software. The Student t-test and Mann-Whitney U test were used to make comparisons between parametric and non-parametric data, respectively. One-way ANOVA and Kruskal–Wallis tests were used to make multi-comparisons between parametric and non-parametric data, respectively. The appropriate test for each experiment is reported in the figure legend. Bars on graphs show 95% confidence intervals.

## *Results*

### Canonical Wnt signalling is active at regions of high strain in the zebrafish lower jaw

Finite Element (FE) models mapping the location of strains acting on the zebrafish lower jaw during mouth opening and closure [11], were utilised to identify signalling activity in areas of high strain. High levels of tensile (Fig 1A) and compressive (Fig 1A') strains from mouth opening muscles are exerted at the anterior of the Meckel's cartilage (MC) and at the outer region of the jaw joint. During mouth closure muscle activity, high strain is located across the jaw joint interzone (Fig 1B, B'). The canonical Wnt reporter line *Tg(7xTCF.XlaSiam:nlsGFP),* [40], reveals cells responding to Wnt are located surrounding the lower jaw at 5dpf (Fig 1A''), with a heterogeneous population of GFP-positive (GFP+) cells surrounding the anterior Meckel's cartilage (MC) and the jaw joints (Fig 1A'',B''). This localisation of GFP-positive cells shows a strong spatiotemporal correlation with regions of the jaw experiencing high strain.

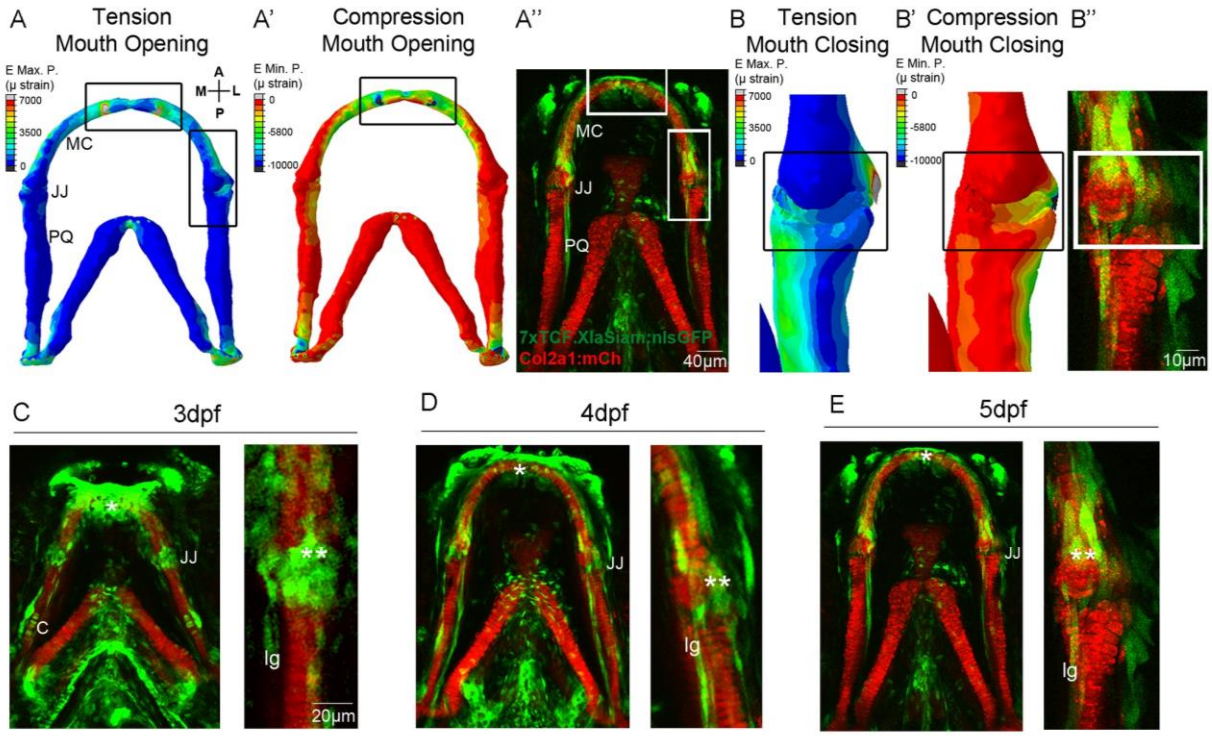


**Fig 1. Patterns of biomechanical strain and location of Wnt responsive cells at the zebrafish lower jaw between 3-5dpf.** (A,A'): Finite Element (FE) model of maximum (E max. P., tension, A) and minimum (E min P., compression, A') Principal strain on the zebrafish lower jaw during mouth opening at 5dpf (application of Intermandibularis and protractor hyoideus). (B,B'): Finite Element (FE) model of maximum (E max. P., tension, B) and minimum (E min P., compression, B') Principal strain on the jaw joint during mouth closure at 5dpf (application of adductor mandibulae). Colour key represents strain calculated in microstrain (μstrain). (A'',B'',C-E): *Tg(7xTCF.XlaSiam:nlsGFP)* and *Tg(Col2a1aBAC:mcherry)* transgenic zebrafish lines labelling Wnt responsive cells and cartilage of the lower jaw, respectively at 3 (C), 4 (D) and 5dpf (A'',B'',E). (C-E): left hand panel: lower jaw, right hand panel and (B''): jaw joint. (A,A') and (B,B') have been reproduced from the previously published paper under a Creative Commons Licence [11]. A= anterior, P= posterior, M=medial, L= lateral, MC= Meckel's Cartilage, JJ= jaw joint, PQ=palatoquadrate, C= cartilage, lg=ligament, *= anterior MC, **= jaw joint.

We therefore studied jaw expression of the Wnt reporter from 3-5 dpf, a time which we have previously identified as critical for normal joint morphogenesis [11]. Using morphology, location and immunohistochemical labelling against ligament and tendon, and chondrocyte markers we identified a heterogeneous population of GFP+ cells (S2 Fig), which included: chondrocytes at the jaw joint (S2A Fig) and along the palatoquadrate (PQ) (Fig 1C, c) and ligaments and tendon (Fig 1C-E, S2B Fig). Additional GFP+ cells surrounding the jaw joints (Fig 1C-E, **) were identified as perichondrial joint-associated cells. These Wnt responsive cells at the lower jaw are, therefore, not only located in areas subjected to high levels of tensile and compressive strain but include cell types known to respond to biomechanical stimuli such as chondrocytes and ligaments.

**Canonical Wnt signalling at the lower jaw is biomechanically controlled**

To test whether canonical Wnt signalling in the jaw is mechanically controlled, zebrafish carrying transgenes for *Col2a1aBAC:mcherry* and *7xTCF.XlaSiam:nlsGFP* were immobilised from 3-5dpf to prevent jaw movement, and *Tg(7xTCF.XlaSiam:nlsGFP)* GFP+ signal was quantified by measuring the volume of segmented GFP+ cells within a region of interest at the lower jaw (Fig 2). A significantly reduced GFP+ signal at the lower jaw at 5dpf was present after a period of immobilisation, most notably at the jaw joint region (Fig 2A,B), as shown by 3D render of the green channel in the area surrounding the jaw joint and PQ. At 5dpf, the volume of GFP+ signal surrounding the MC joint and PQ (Fig 2C), and specifically at the jaw joint (Fig 2D), was significantly reduced in immobilised zebrafish (Fig 2C',D'). The total number of GFP+ Wnt responsive cells in the jaw joint region was significantly reduced at 5dpf (Fig 2E,F) and there were significantly fewer GFP+ ligament/tendon cells at 4 and 5dpf (Fig 2G). This demonstrates that loss of muscle activity affects canonical Wnt activity at the lower jaw, suggesting that Wnt signalling is biomechanically controlled.

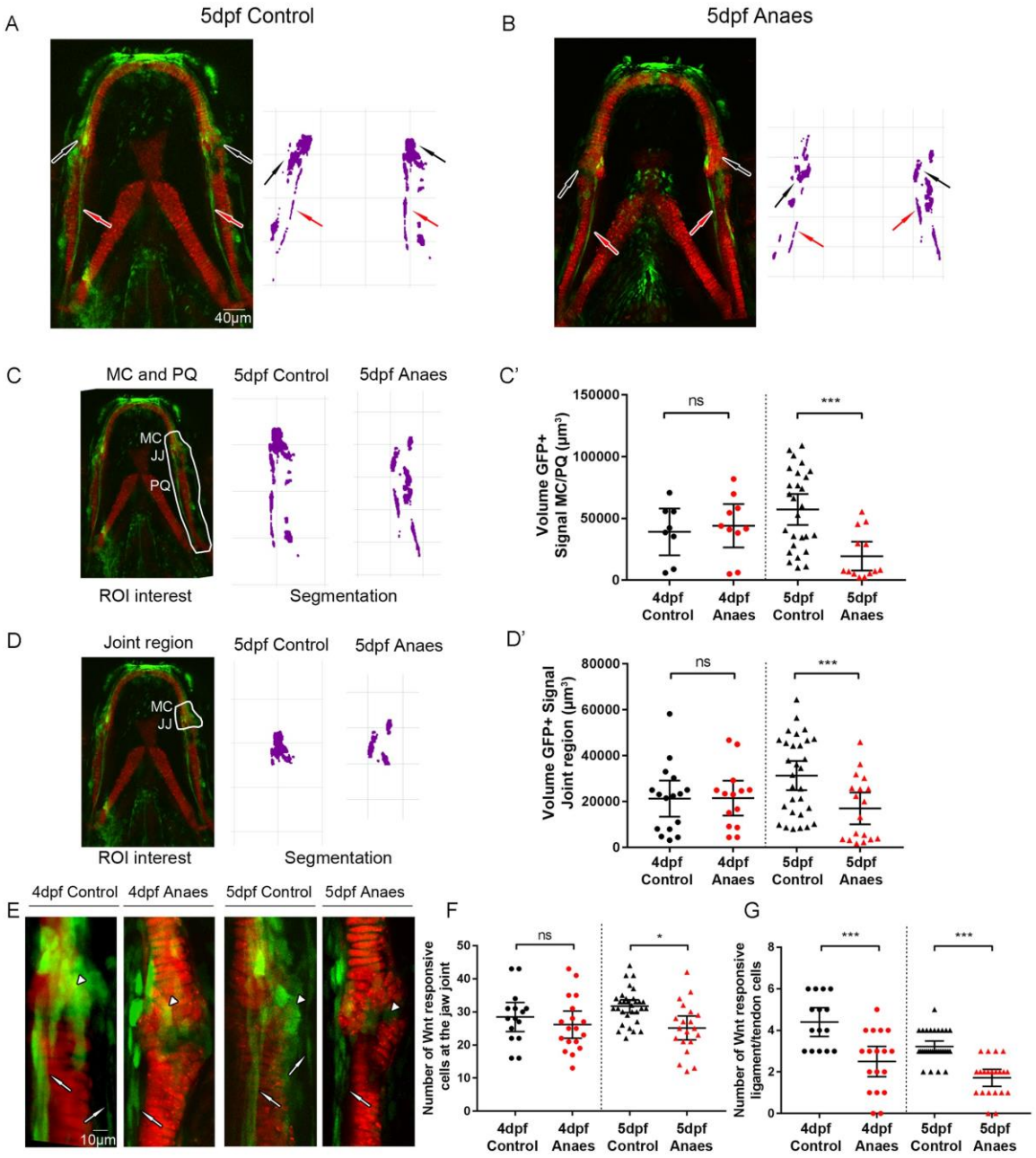


284

285 **Fig 2. Immobilisation causes a reduction in canonical Wnt signalling activity at the zebrafish lower**

286 **jaw.** (A,B): *Tg(7xTCF.XlaSiam:nlsGFP)* and *Tg(Col2a1aBAC:mcherry)* transgenic zebrafish lines were used to

287 visualise Wnt responsive cells and chondrocytes, respectively in 5dpf control (A) and 5dpf 3-5dpf immobilised

288 (B) zebrafish. Left panel= merge of *Tg(7xTCF.XlaSiam:nlsGFP)* and *Tg(Col2a1aBAC:mcherry)*. Right panel=

289 Segmentation of GFP signal. Black arrows= Cells surrounding jaw joint, red arrows= ligaments and tendons. (C):

290 Left panel: volume analysis of *Tg(7xTCF.XlaSiam:nlsGFP)* GFP-positive (GFP+) signal at the region of interest

291 (ROI): from 6 intercalating cells above the Meckel's Cartilage (MC) jaw joint and along the full extent of the

292 palatoquadrate (PQ) (white line). Right panel: Segmentation of GFP+ signal volume from region of interest in
293 5dpf control and anesthetised zebrafish. (C'): Volume ($\mu m^3$) of GFP+ signal at the MC joint and along the PQ in
294 4 and 5dpf control and anaesthetised zebrafish. (n=8, 10, 27, 13). (D): Left panel: volume analysis of
295 *Tg(7xTCF.XlaSiam:nlsGFP)* GFP-positive (GFP+) signal at the ROI from 6 intercalating cells above the Meckel's
296 Cartilage (MC) jaw joint to the interzone (white line). Right panel: Segmentation of GFP+ signal volume from
297 region of interest in 5dof control and anaesthetised zebrafish. (D'): Volume ($\mu m^3$) of GFP+ signal at the MC
298 joint in 4 and 5dpf control and anaesthetised zebrafish. (n=16, 14, 30, 18). (E): *Tg(7xTCF.XlaSiam:nlsGFP)* and
299 *Tg(Col2a1aBAC:mcherry)* transgenic zebrafish mark Wnt responsive cells and cartilage of the lower jaw at the
300 jaw joint in 4 and 5dpf control and anaesthetised zebrafish. White arrowheads indicate joint-associated GFP+
301 cells. White arrows indicate ligament and tendon GFP+ cells. (F): Number of GFP+ cells in 4 and 5dpf control
302 and anaesthetised zebrafish in a 50x80µm area surrounding the jaw joint. (n=15, 18, 31, 13). (G): Number of
303 ligament and tendon GFP+ cells in 4 and 5dpf control and anaesthetised zebrafish at the jaw joint. (n=15, 18,
304 31, 13). Kruskal-Wallis tests were performed for statistical analysis in (C',D',G) and one-way ANOVA in (F). ns=
305 not significant, *=p≤0.05, **=p≤0.01, ***=p≤0.001.

306

307 **Blocking canonical Wnt signalling leads to altered jaw joint morphology independent of muscle**
308 **activity**

309 We have previously shown that immobilising the jaw leads to abnormal joint formation [11, 12]. To
310 test whether changes to Wnt activity affect jaw joint morphology, independent of movement,
311 *Tg(Col2a1aBAC:mcherry)* zebrafish were exposed to the Wnt antagonist, IWR-1, from 3-5dpf. The
312 addition of IWR-1 had no significant effect on the frequency of mouth movements compared to
313 control (S3 Fig), i.e. jaw muscle activity was normal. However, IWR-1 treatment affects the
314 functional morphology of the 5dpf jaw joint, such that the medial region of the MC overlapped the
315 PQ element, impeding smooth movement (Fig 3A,A'). IWR-1 treatment caused the lateral interzone
316 region to be significantly larger than control and the medial interzone region to be significantly
317 reduced due to overlapping elements (Fig 3B-B'). There was no effect on the total length of the jaw

318 (S4A Fig) or MC (S4B Fig), suggesting that normal growth was not inhibited. However, the proportion
319 of chondrocytes in the MC that were fully intercalated was significantly reduced (S4C Fig),
320 concurrent with a significant increase in the proportion of rounded chondrocytes at the 5dpf jaw
321 joint (S4D Fig). This failure of intercalation and reduced cell maturation at the joint phenocopies
322 what is previously seen in immobilised *nic* b107 mutants and anaesthetised zebrafish [10, 12].
323 Therefore, IWR-1 treatment, independent of muscle activity and joint movement, recapitulates cell
324 behaviours seen after immobility.

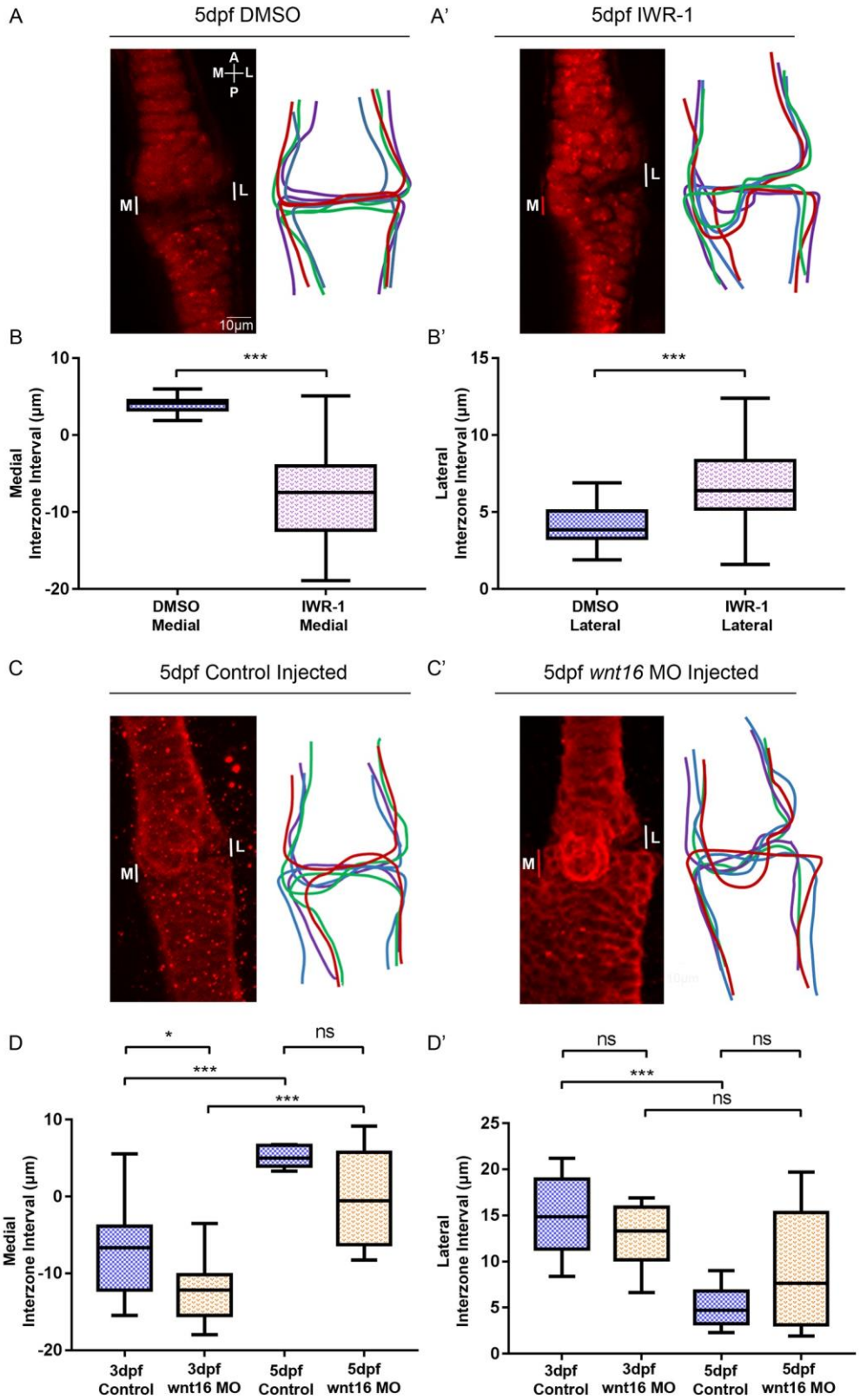


325

326 **Fig 3. Manipulation of Wnt affects zebrafish jaw joint morphology.** (A-A'): 5dpf DMSO control (A) and

327 20µM IWR-1 treated (A') zebrafish jaw joint morphology. Left panels: *Tg(Col2a1aBAC:mcherry)* transgenic

zebrafish line marks cartilage of the jaw joint. Right panels: Outlines of 4 representative jaw joints. A= Anterior, P= Posterior, M= Medial, L= Lateral. White lines= Interzone Interval measurements between MC and PQ, red line= Overlapping Interval between MC and PQ. (B-B'): Interzone intervals (µm) between the MC and PQ on the medial (B) and lateral (B') regions of the jaw joint in 5dpf DMSO and IWR-1 treated zebrafish. Negative values represent an overlap of MC/PQ elements. (n=42, 45). Two-tailed student t-tests were performed for (B,B'). (C-C'): 5dpf control injected (C) and Wnt16 morpholino (MO) injected (C') zebrafish jaw joint morphology. Left panels: Immunohistochemical stain of the jaw joint region. Right panels: Outlines of 4 representative jaw joints. (D-D'): Interzone intervals (µm) between the MC and PQ on the medial (D) and lateral (D') regions of the jaw joint in 5dpf control injected and Wnt16 MO injected zebrafish. Negative values represent an overlap of MC/PQ elements. (n=8, 11, 6, 8). One-way ANOVAS were performed (D,D'). ns= not significant, *=p≤0.05, **=p≤0.01, ***=p≤0.001.

**Knockdown of Wnt16 leads to altered jaw joint morphology**

Application of a Wnt antagonist (IWR-1) shows that a reduction in canonical Wnt activity leads to abnormal jaw joint morphogenesis. We took a candidate approach to identify Wnt pathway members that could transduce the mechanical signal into altered cell behaviour. Wnt16 has been previously reported to be expressed in mouse limb joints [36], differentially regulated in mice lacking limb muscle [35] and Wnt16 overexpression in mouse joint synovium has been shown to activate canonical Wnt signalling in joint cartilage [53]. In zebrafish, Wnt16 is required to control notch signalling for haematopoietic stem cell specification [51]. We used the previously described Wnt16 MO, [51], to determine the effect of reduced Wnt16 on jaw and joint morphology. Wnt16 knockdown had no effect on the gross morphology of the zebrafish larvae (S1B Fig) or on frequency of jaw movement (data not shown). Wnt16 knockdown led to reduced levels of *lef1* mRNA in jaw cartilage elements such as the branchial arches (S5A,A' Fig), whilst leaving other expression domains - such as the brain - intact (S5A,A' Fig). Wnt16 morphants showed a significant reduction in *Tg(7xTCF.XlaSiam:nlsGFP)* GFP+ signal volume in the jaw compared to control (S5B-E Fig),

354 demonstrating that Wnt16 activates canonical Wnt signalling in the lower jaw independent of jaw
355 movement.

356 Wnt16 morphants show altered jaw joint morphology with an overlapping MC element (Fig 3C-C').
357 At 3dpf, Wnt16 morphants have a reduced interzone space on the medial side of the joint due to the
358 overlap of the elements on the medial side (Fig 3D-D'). Interzone interval measurements were,
359 however, not significantly different to control at 5dpf. This shows Wnt16 knockdown affects
360 functional jaw joint morphology, but is less severe than IWR-1 treated fish at 5dpf. Wnt16 MO
361 injection did not significantly affect the total jaw length or MC length at 5dpf, showing that overall
362 jaw growth was unaffected and Wnt16 knockdown very specifically affects only the joint region of
363 the cartilage element (S4A,B Fig), with no other discernible off-target effects. Unlike IWR-1
364 treatment, Wnt16 knockdown does not significantly affect cell intercalation (S4C,D Fig). Therefore,
365 Wnt16 is important for joint morphology, but does not affect cell intercalation.

366 **Cell proliferation, migration and changes to cell morphology contribute to jaw joint**
367 **morphogenesis**

368 In order to understand the cell behaviour changes that shape the joint, we tracked cells at the joint
369 in individual larvae. As continuous time lapse imaging to follow the process of joint morphogenesis
370 would require long-term immobilisation; which would in turn lead to abnormal morphogenesis, we
371 used zebrafish carrying both *Tg(Sox10:GAL4-VP16)* and *Tg(UAS:Kaede)* transgenes to track
372 populations of kaede-expressing joint cells from 3 to 5dpf. A small batch of 10-12 cells at the medial
373 side of the joint were photoconverted at 3dpf to irreversibly switch the labelling from green to red,
374 making it possible to follow the cells over time. Medially located cells close to the retroarticular
375 process (RAP) were chosen as the medial region of the joint is most affected morphologically by
376 immobilisation and Wnt abrogation (Fig 3, [11]). Red photoconverted cells located at the medial side
377 of the joint at 3dpf spread along the anterior-posterior axis of the jaw joint by 5dpf, contributing to
378 the change in joint shape (Fig 4A,C). Some of the cells within this group remain part of the MC;

however other cells migrate to the PQ element. Between 3 and 5dpf there is a 97.5% mean increase in the area occupied by red cells at the joint (Fig 4E). Cell counts reveal that this increase in area, in part, is due to an increase in cell number from 3-5dpf (Fig 4F), showing that proliferation contributes to changes in joint shape. BrdU pulse chase experiments show that proliferation events mainly take place between 4 and 5dpf (S6A-A'',D Fig). From 3 to 5dpf, cell morphology changes are also observed, with elongated perichondrial cells migrating from the original pool of round photoconverted cells to form the perichondrium (Fig 4A,C). These data demonstrate that cells at the joint are highly dynamic, with migration, proliferation and changes to cell type and morphology all contributing to normal joint morphogenesis.

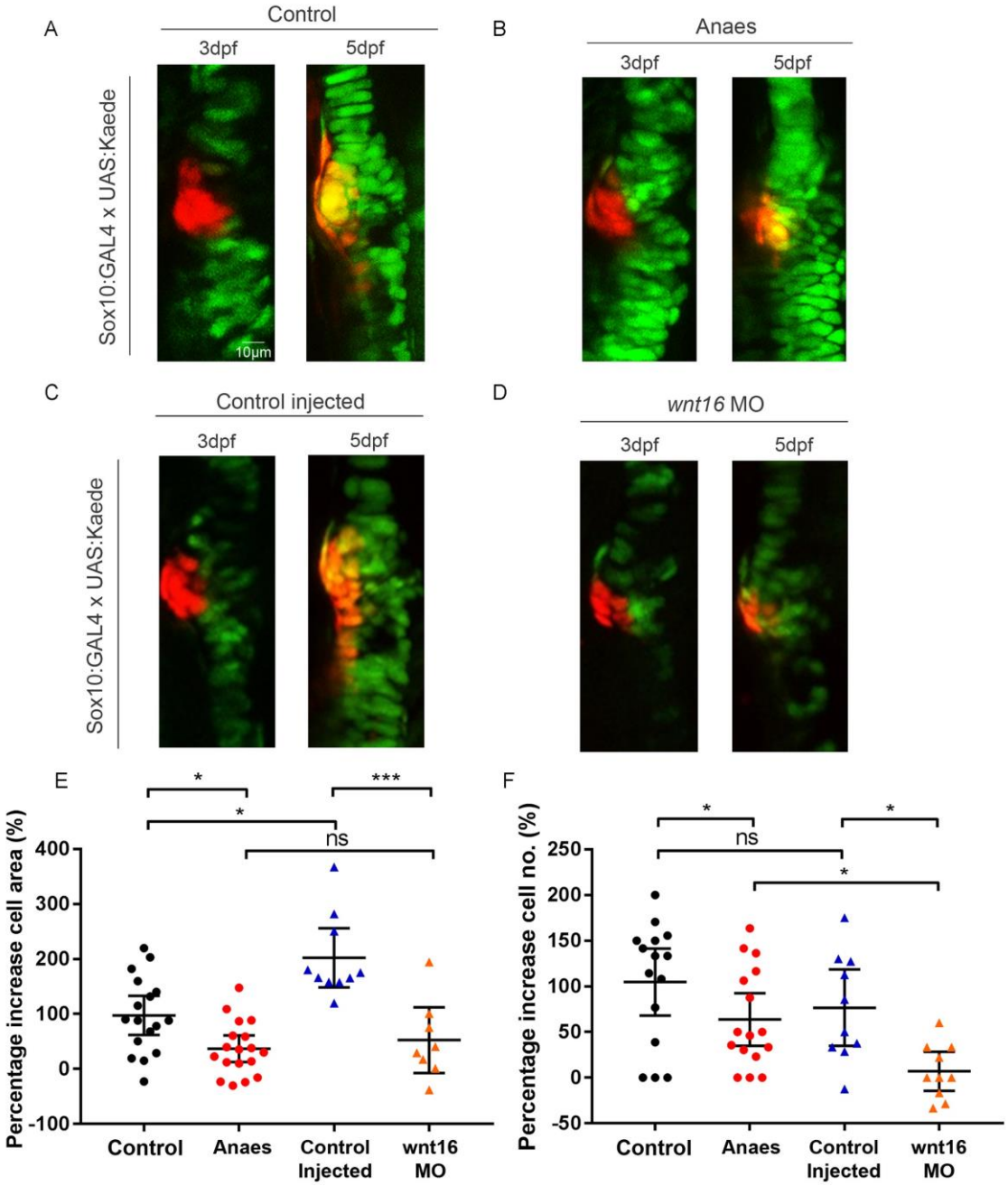


388

389 **Fig 4. Immobilisation and Wnt16 knockdown affects cell proliferation and migration at the medial**

390 **region of the jaw joint between 3-5dpf.** (A-D): *Tg(Sox10:GAL4-VP16)* and *Tg(UAS:Kaede)* transgenic line

391 drives expression of kaede protein (green) in cartilage of control (A), anaesthetised (B), control injected (C) and

392 Wnt16 morpholino (MO) injected (D) zebrafish. At the jaw joint, medially located kaede expressing cells are

393 photoconverted to red kaede at 3dpf (left panels). Right panels show jaw joints from the same larva reimaged

394 at 5dpf. Photoconverted cells appear red/orange due to presence of photoconverted red kaede and

expression of newly made green kaede protein under control of sox10 promoter. (E): Percentage increase in total area of cells expressing photoconverted red kaede between 3 and 5dpf in control, anaesthetised, control injected and Wnt16MO injected zebrafish jaw joints. (n=17, 18, 10, 8). (F): Percentage increase in number of cells expressing photoconverted red kaede between 3 and 5dpf in control, anaesthetised, control injected and Wnt16MO injected zebrafish jaw joints. (n=15, 16, 10, 10). Kruskal-Wallis tests were performed for (E,F). ns= not significant, *=p≤0.05, **=p≤0.01, ***=p≤0.001.

We then tracked cells at the joint in immobilised larvae to investigate whether cell behaviour is altered in these larvae. In immobilised larvae, the location of red photoconverted cells remained largely static between 3 and 5dpf (Fig 4B) and the percentage increase in the area occupied by red cells was significantly reduced compared to control (Fig 4E). The percentage increase in the number of cells inheriting red kaede at the joint between 3 and 5 dpf was also significantly reduced (Fig 4F). This demonstrates that immobilisation has an effect on cell behaviours including migration and proliferation. Therefore, mechanical stimuli are required to trigger normal cell behaviours such as proliferation and migration in order to correctly shape the joint.

**Wnt16 controls cell proliferation and migration at the jaw joint**

To investigate whether Wnt16 plays a role in controlling cell behaviours at the joint, a group of 10-12 red photoconverted cells per fish were tracked in Wnt16 morphants. From 3 to 5dpf, the spread of red photoconverted cells observed in control injected larvae did not take place in Wnt16 morphants (Fig 4C,D). The percentage increase in area taken up by red cells was significantly reduced in morphants compared to control larvae reflecting this failure to change cell location from 3 to 5dpf (Fig 4D,E). The percentage increase in cell number was significantly reduced compared to control (Fig 4F) and the number of BrdU positive cells at the joint was also significantly less (S6C,D Fig). This shows that Wnt16 controls cell behaviours including proliferation and migration during joint morphogenesis. Interestingly, the effect of Wnt16 knockdown on chondrocyte migration and

proliferation is joint specific, as there was no significant change in cell behaviour when cells of the intercalated region of the element were tracked (S6B',C',E Fig, S7 Fig), which again confirms specificity of the MO.

Next, we used zebrafish with the *ubi:Zebrabow* transgene under the control of *Sox10:cre* to track individual cells of different colours at the joint, in order to unpick individual cell behaviours taking place during joint morphogenesis. At 3dpf, the retroarticular process (RAP) of the jaw joint contains cells of different shades, which could be tracked (Fig 5A-A''). In control zebrafish, cells that had undergone proliferation between 3-5dpf were observed at the joint (Fig 5B, duplicated white and green asterisks). Cell morphology changes were also observed (Fig 5B', yellow and blue outlined cells), showing that a combination of proliferation and changes to cell morphology contribute to the overall change in joint shape.

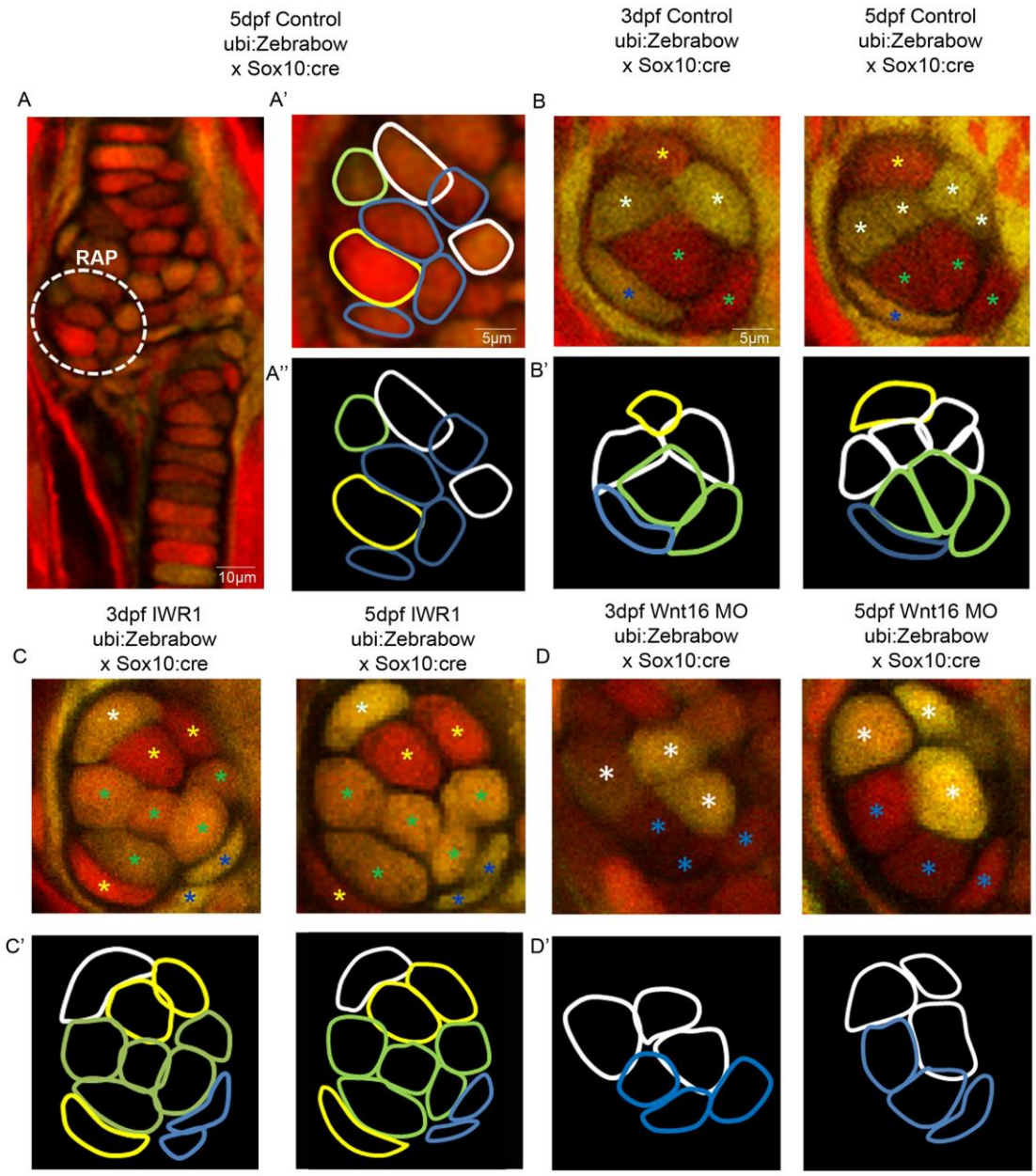


**Fig 5. Wnt manipulation affects cell proliferation and cell morphology at the jaw joint revealed using Zebrabow transgenic line.** (A-A''): *Tg(ubi:Zebrabow)* and *Tg( Sox10:cre)* transgenic lines generate multiple colours of fluorescence in zebrafish cartilage including at the region of interest at the Retroarticular process (RAP), (white dotted line). Cell outlines were created at the RAP (A': RAP cell outlines overlay with confocal image, A'': cell outlines). A=anterior, P=posterior, M=medial, L=lateral. (B, C, D): 3 and 5dpf *Tg(ubi:Zebrabow)* and *Tg( Sox10:cre* control (B), IWR-1 treated (C) and Wnt16 MO injected zebrafish (D). The Retroarticular process (RAP) of the MC jaw joint is shown. Asterisks of different colours mark cells at 3 and

5dpf (indicating re-identification and cell division events). (B', C', D'): Outlines of individual cells in the RAP of the MC jaw joint, identified in Control (B'), IWR-1 treated (C') and Wnt16 MO injected (D') *Tg(ubi:Zebrabow)* and *Tg( Sox10:cre)* transgenic zebrafish. Outline colour of individual cells in (B', C', D') matches asterix colour in (B, C, D).

However, in IWR-1 treated and Wnt16 morphant larvae, cell proliferation was not observed in the RAP of the jaw joint between 3-5dpf (Fig 5C-D). In IWR-1 treated zebrafish the cells of the RAP are less plastic, with minimal changes to cell morphology between 3-5dpf (Fig 5C'). In Wnt16 morphants, cell morphology changes were not affected, as the cells of the RAP became larger or changed shape (Fig 5D', e.g. lower blue cell). This shows that normal joint morphogenesis requires cell proliferation and changes to individual cell morphology. Both cellular processes are affected by IWR-1 application and proliferation is affected by Wnt16MO knockdown. This shows that Wnt16 controls cell proliferation and migration at the joint, but suggests that cell morphology changes must be controlled by other members of the Wnt pathway.

## ***Discussion***

Mechanical input has previously been shown to affect joint morphogenesis in a number of species ranging from mouse to fish [1-3, 11, 12]. However, which downstream signalling pathways drive the cell behaviours that shape the joint in response to these forces is less well characterised. By tracking cell behaviour dynamically in the joint for the first time in larvae subjected to mechanical, genetic and pharmacological perturbations, we show that joint morphology is shaped through a combination of cell morphology changes, migration and proliferation. Cells at the medial region of joint; most affected in mechanical loss models, normally spread and migrate anterior and posterior to their original location to remain part of the Meckel's cartilage or become part of the palatoquadrate. Cell proliferation at the jaw joint mainly occurs from 4 to 5dpf and cell morphology changes also contribute to the overall shape of the joint. We also show that interzone cells can give

464 rise to mature chondrocytes or can form part of the perichondrium. This is the first study to describe
465 the dynamic cell behaviours occurring at the joint in individually tracked animals and therefore gives
466 an insight into morphogenesis of the joint *in vivo*. We show that removal of muscle force leads to
467 reduced proliferation in the zebrafish joint, analogous to the situation in chicks and mice [3, 22, 23].
468 Our work also builds on previous work showing the relevance of the zebrafish as a model for
469 synovial joint development [54].

470 Here, we demonstrate that canonical Wnt signalling, and Wnt16 act downstream of muscle activity
471 to transduce the mechanical signals into the cell behavioural changes, such as proliferation and
472 migration, that shape the joint. It has been previously shown in mesenchymal stem cell *in vitro*
473 preparations that mechanical strain can activate Wnt signalling [35, 37, 38] and transcriptomic
474 studies in muscle-less mice have demonstrated changes in expression levels of Wnt pathway
475 members [35]. We show that canonical Wnt signalling is activated in cells associated with the
476 zebrafish jaw joint, such as chondrocytes and ligaments, which are located in regions under high
477 levels of strain. We demonstrate that canonical Wnt signalling in the jaw joint, and in ligaments is
478 mechanosensitive, with significant reductions to the number Wnt GFP+ positive cells at the joint and
479 in associated connective tissues when force is lost. Previous work in zebrafish has shown that
480 craniofacial muscle is not required for induction of expression of early markers of tendon and
481 ligament, but that muscle attachment is required for maintenance of expression at 72hpf [24].
482 Immobilisation in our study starts somewhat later (from 72hpf) but we can still identify changes to
483 cell behaviour in the ligaments and a reduction of Wnt signal activity at 4 and 5dpf. This strongly
484 suggests that canonical Wnt signalling plays a role in later tendon and ligament maturation, which
485 requires mechanical input. Wnt/B-catenin has been linked to a mechanosensitive role in controlling
486 expression of osteogenic genes in cells derived from human periodontal ligaments [55, 56], and our
487 work would suggest that Wnt is likely to play a role in maturation of other craniofacial ligaments. We
488 observe that canonical Wnt signalling manipulation causes abnormalities in joint morphology. This

489 occurs even in conditions where muscle activity is still present, demonstrating that that Wnt
490 signalling acts downstream of muscle activity to cause changes in joint shape.

491 We show that Wnt16 is important for accurate shaping of the joint by controlling cell proliferation
492 and migration events at the joint. Unlike reduction in broad canonical Wnt signalling, abrogation of
493 Wnt16 had no effect on cell behaviours such as proliferation, migration and intercalation of
494 maturing chondrocytes anterior to the jaw joint, acting in a highly joint specific fashion. Therefore,
495 other Wnt ligands are likely to be responsible for chondrocyte intercalation in the Meckel's cartilage,
496 as is the case for chondrocyte intercalation in chick growth plates [57, 58] and during zebrafish
497 palate morphogenesis [58-60]. Wnt16 has been previously implicated in joint formation, bone
498 homeostasis and remodelling [31, 61, reviewed in 62] and is expressed at the developing joint in
499 mouse models [31, 36]. It has been shown to be required for proliferation, differentiation and
500 specification in other cell types such as haematopoietic stem cells, osteoclasts, osteoblasts and
501 keratinocytes [51, 63-65]. Wnt16 is upregulated following mechanical injury in *ex vivo* human
502 cartilage [66], and following mechanical loading of the tibia in mice [67]. Expression levels of Wnt16
503 were upregulated in 'muscleless' *Splotch* mice compared to control [35, 66, 67]. We show that
504 Wnt16 controls proliferation and migration of a small number of cells in the joint, which are critical
505 for normal joint morphology to be generated.

506 The role of Wnts; in particular Wnt16, by controlling joint morphogenesis during development may
507 have a longer term impact on joint health The formation of abnormal joint morphology during
508 development is a critical risk factor in onset of osteoarthritis [Reviewed in 68]. Wnt-related genes
509 such as Wnt antagonist FRZB are implicated in accurate joint shaping [69]. Wnt16 has been linked
510 with the relationship between hip geometry and risk of osteoarthritis onset [70]. Wnt16 is
511 upregulated in joints with moderate to severe OA along with increased nuclear beta-catenin
512 expression [66]. Upregulation is also documented after mechanical injury [66]. Our study builds on

513 these findings to suggest that the relationship found between OA risk, joint shape and Wnt16 may
514 stem from its role in activating early joint cell behaviours that affect the functional joint shape.

515 ***Acknowledgements***

516 The authors would like to thank members of the Wolfson Bioimaging facility for their imaging
517 acquisition expertise and Dominic Alibhai for Multiphoton microscopy support. We would also like to
518 thank Robert Knight for supply of plasmids and Karen Roddy and members of the Hammond lab for
519 discussions during the preparation of the manuscript.

1. Nowlan NC, Sharpe J, Roddy KA, Prendergast PJ, Murphy P. Mechanobiology of Embryonic Skeletal Development: Insights from Animal Models. Birth Defects Research Part C-Embryo Today-Reviews. 2010;90(3):203-13.
2. Rolfe R, Roddy K, Murphy P. Mechanical Regulation of Skeletal Development. Current Osteoporosis Reports. 2013;11(2):107-16.
3. Kahn J, Shwartz Y, Blitz E, Krief S, Sharir A, Breitel DA, et al. Muscle Contraction Is Necessary to Maintain Joint Progenitor Cell Fate. Developmental Cell. 2009;16(5):734-43.
4. Gomez C, David V, Peet NM, Vico L, Chenu C, Malaval L, et al. Absence of mechanical loading in utero influences bone mass and architecture but not innervation in Myod-Myf5-deficient mice. Journal of Anatomy. 2007;210(3):259-71.
5. Nowlan NC, Bourdon C, Dumas G, Tajbakhsh S, Prendergast PJ, Murphy P. Developing bones are differentially affected by compromised skeletal muscle formation. Bone. 2010;46(5):1275-85.
6. Rot-Nikcevic I, Reddy T, Downing KJ, Belliveau AC, Hallgrimsson B, Hall BK, et al. Myf5(-/-): MyoD(-/-) amyogenic fetuses reveal the importance of early contraction and static loading by striated muscle in mouse skeletogenesis. Development Genes and Evolution. 2006;216(1):1-9.
7. Rot-Nikcevic I, Downing KJ, Hall BK, Kablar B. Development of the mouse mandibles and clavicles in the absence of skeletal myogenesis. Histology and Histopathology. 2007;22(1):51-60.
8. Murray PDF, Selby D. Intrinsic and extrinsic factors in the primary development of the skeleton. Wilhelm Roux Archiv Fur Entwicklungsmechanik Der Organismen. 1930;122(3):629-62.
9. Roddy KA, Nowlan NC, Prendergast PJ, Murphy P. 3D representation of the developing chick knee joint: a novel approach integrating multiple components. Journal of Anatomy. 2009;214(3):374-87.
10. Shwartz Y, Farkas Z, Stern T, Aszodi A, Zelzer E. Muscle contraction controls skeletal morphogenesis through regulation of chondrocyte convergent extension. Developmental Biology. 2012;370(1):154-63.
11. Brunt LH, Norton JL, Bright JA, Rayfield EJ, Hammond CL. Finite element modelling predicts changes in joint shape and cell behaviour due to loss of muscle strain in jaw development. J Biomech. 2015.
12. Brunt LH, Skinner REH, Roddy KA, Araujo NM, Rayfield EJ, Hammond CL. Differential effects of altered patterns of movement and strain on joint cell behaviour and skeletal morphogenesis. Osteoarthritis and Cartilage. 2016;24(11):1940-50.
13. Shea CA, Rolfe RA, Murphy P. The importance of foetal movement for co-ordinated cartilage and bone development in utero : clinical consequences and potential for therapy. Bone Joint Res. 2015;4(7):105-16.
14. Nayak SS, Kadavigere R, Mathew M, Kumar P, Hall JG, Girisha KM. Fetal Akinesia Deformation Sequence: Expanding the Phenotypic Spectrum. American Journal of Medical Genetics Part A. 2014;164(10):2643-8.
15. Luterkort M, Persson PH, Polberger S, Bjerre I. HIP-JOINT INSTABILITY IN BREECH PREGNANCY. Acta Paediatrica Scandinavica. 1986;75(5):860-3.
16. Clarke NMP. Swaddling and hip dysplasia: an orthopaedic perspective. Archives of Disease in Childhood-Fetal and Neonatal Edition. 2014;99(1):5-U26.
17. Sugano N, Noble PC, Kamaric E, Salama JK, Ochi T, Tullos HS. The morphology of the femur in developmental dysplasia of the hip. Journal of Bone and Joint Surgery-British Volume. 1998;80B(4):711-9.
18. Mavcic B, Iglic A, Kralj-Iglic V, Brand RA, Vengust R. Cumulative hip contact stress predicts osteoarthritis in DDH. Clinical Orthopaedics and Related Research. 2008;466(4):884-91.
19. Grad S, Eglin D, Alini M, Stoddart MJ. Physical Stimulation of Chondrogenic Cells In Vitro: A Review. Clinical Orthopaedics and Related Research. 2011;469(10):2764-72.
20. Chen JH, Liu C, You LD, Simmons CA. Boning up on Wolff's Law: Mechanical regulation of the cells that make and maintain bone. Journal of Biomechanics. 2010;43(1):108-18.

570 21. Nowlan NC, Prendergast PJ, Murphy P. Identification of Mechanosensitive Genes during
571 Embryonic Bone Formation. Plos Computational Biology. 2008;4(12):10.
572 22. Jahan E, Matsumoto A, Rafiq AM, Hashimoto R, Inoue T, Udagawa J, et al. Fetal jaw
573 movement affects Ihh signaling in mandibular condylar cartilage development: The possible role of
574 Ihh as mechanotransduction mediator. Archives of Oral Biology. 2014;59(10):1108-18.
575 23. Roddy KA, Prendergast PJ, Murphy P. Mechanical Influences on Morphogenesis of the Knee
576 Joint Revealed through Morphological, Molecular and Computational Analysis of Immobilised
577 Embryos. Plos One. 2011;6(2).
578 24. Chen JW, Galloway JL. The development of zebrafish craniofacial tendon and ligament
579 progenitors. American Journal of Medical Genetics Part A. 2014;164(8):1879-80.
580 25. Chen JW, Galloway JL. Using the zebrafish to understand tendon development and repair.
581 Methods Cell Biol. 2017;138:299-320.
582 26. Niehrs C. The complex world of WNT receptor signalling. Nature Reviews Molecular Cell
583 Biology. 2012;13(12):767-79.
584 27. Willert K, Nusse R. Wnt Proteins. Cold Spring Harbor Perspectives in Biology. 2012;4(9):13.
585 28. Church V, Nohno T, Linker C, Marcelle C, Francis-West P. Wnt regulation of chondrocyte
586 differentiation. Journal of Cell Science. 2002;115(24):4809-18.
587 29. Hartmann C, Tabin CJ. Dual roles of Wnt signaling during chondrogenesis in the chicken limb.
588 Development. 2000;127(14):3141-59.
589 30. Yang YZ, Topol L, Lee H, Wu JL. Wnt5a and Wnt5b exhibit distinct activities in coordinating
590 chondrocyte proliferation and differentiation. Development. 2003;130(5):1003-15.
591 31. Guo XZ, Day TF, Jiang XY, Garrett-Beal L, Topol L, Yang YZ. Wnt/beta-catenin signaling is
592 sufficient and necessary for synovial joint formation. Genes & Development. 2004;18(19):2404-17.
593 32. Hartmann C, Tabin CJ. Wnt-14 plays a pivotal role in inducing synovial joint formation in the
594 developing appendicular skeleton. Cell. 2001;104(3):341-51.
595 33. Ikegawa M, Han H, Okamoto A, Matsui R, Tanaka M, Omi N, et al. Syndactyly and preaxial
596 synpolydactyly in the single Sfrp2 deleted mutant mice. Developmental Dynamics.
597 2008;237(9):2506-17.
598 34. Pazin DE, Gamer LW, Cox KA, Rosen V. Molecular profiling of synovial joints: Use of
599 microarray analysis to identify factors that direct the development of the knee and elbow.
600 Developmental Dynamics. 2012;241(11):1816-26.
601 35. Rolfe RA, Nowlan NC, Kenny EM, Cormican P, Morris DW, Prendergast PJ, et al. Identification
602 of mechanosensitive genes during skeletal development: alteration of genes associated with
603 cytoskeletal rearrangement and cell signalling pathways. Bmc Genomics. 2014;15:23.
604 36. Witte F, Dokas J, Neuendorf F, Mundlos S, Stricker S. Comprehensive expression analysis of
605 all Wnt genes and their major secreted antagonists during mouse limb development and cartilage
606 differentiation. Gene Expression Patterns. 2009;9(4):215-23.
607 37. Arnsdorf EJ, Tummala P, Jacobs CR. Non-Canonical Wnt Signaling and N-Cadherin Related
608 beta-Catenin Signaling Play a Role in Mechanically Induced Osteogenic Cell Fate. Plos One.
609 2009;4(4):10.
610 38. Haudenschild AK, Hsieh AH, Kapila S, Lotz JC. Pressure and Distortion Regulate Human
611 Mesenchymal Stem Cell Gene Expression. Annals of Biomedical Engineering. 2009;37(3):492-502.
612 39. Westerfield M. The Zebrafish Book. A Guide for the Laboratory Use of Zebrafish (danio
613 rerio). 4th Edn ed: Univ. of Oregon Press; 2000.
614 40. Moro E, Ozhan-Kizil G, Mongera A, Beis D, Wierzbicki C, Young RM, et al. In vivo Wnt
615 signaling tracing through a transgenic biosensor fish reveals novel activity domains. Developmental
616 Biology. 2012;366(2):327-40.
617 41. Hammond CL, Schulte-Merker S. Two populations of endochondral osteoblasts with
618 differential sensitivity to Hedgehog signalling. Development. 2009;136(23):3991-4000.

42. Lee RTH, Knapik EW, Thiery JP, Carney TJ. An exclusively mesodermal origin of fin mesenchyme demonstrates that zebrafish trunk neural crest does not generate ectomesenchyme. Development. 2013;140(14):2923-32.
43. Hatta K, Tsujii H, Omura T. Cell tracking using a photoconvertible fluorescent protein. Nature Protocols. 2006;1(2):960-7.
44. Pan YA, Freundlich T, Weissman TA, Schoppik D, Wang XC, Zimmerman S, et al. Zebrabow: multispectral cell labeling for cell tracing and lineage analysis in zebrafish. Development. 2013;140(13):2835-46.
45. Rodrigues F, Doughton G, Yang BJ, Kelsh RN. A novel transgenic line using the Cre-lox system to allow permanent lineage-labeling of the zebrafish neural crest. Genesis. 2012;50(10):750-7.
46. Brunt LH, Roddy KA, Rayfield EJ, Hammond CL. Building Finite Element Models to Investigate Zebrafish Jaw Biomechanics. J Vis Exp. 2016(118).
47. Schindelin J, Arganda-Carreras I, Frise E, Kaynig V, Longair M, Pietzsch T, et al. Fiji: an open-source platform for biological-image analysis. Nat Methods. 2012;9(7):676-82.
48. Otsu N. A Threshold Selection Method from Gray-Level Histograms. *IEEE Transactions on Systems, Man, and Cybernetics*; 1979. p. 62-6.
49. Edelsbrunner H, Kirkpatrick DG, Seidel R. On the shape of a set of points in the plane. IEEE Transactions on Information Theory; 1983. p. 551-9.
50. Mutoh T, Miyata T, Kashiwagi S, Miyawaki A, Ogawa M. Dynamic behavior of individual cells in developing organotypic brain slices revealed by the photoconvertable protein Kaede. Experimental Neurology. 2006;200(2):430-7.
51. Clements WK, Kim AD, Ong KG, Moore JC, Lawson ND, Traver D. A somitic Wnt16/Notch pathway specifies haematopoietic stem cells. Nature. 2011;474(7350):220-U62.
52. Thisse C, Thisse B. High-resolution in situ hybridization to whole-mount zebrafish embryos. Nature Protocols. 2008;3(1):59-69.
53. van den Bosch MH, Blom AB, Sloetjes AW, Koenders MI, van de Loo FA, van den Berg WB, et al. Induction of Canonical Wnt Signaling by Synovial Overexpression of Selected Wnts Leads to Protease Activity and Early Osteoarthritis-Like Cartilage Damage. Am J Pathol. 2015;185(7):1970-80.
54. Askary A, Smeeton J, Paul S, Schindler S, Braasch I, Ellis NA, et al. Ancient origin of lubricated joints in bony vertebrates. Elife. 2016;5.
55. Chen LJ, Hu BB, Shi XL, Ren MM, Yu WB, Cen SD, et al. Baicalein enhances the osteogenic differentiation of human periodontal ligament cells by activating the Wnt/beta-catenin signaling pathway. Arch Oral Biol. 2017;78:100-8.
56. Zhang L, Liu W, Zhao J, Ma X, Shen L, Zhang Y, et al. Mechanical stress regulates osteogenic differentiation and RANKL/OPG ratio in periodontal ligament stem cells by the Wnt/beta-catenin pathway. Biochim Biophys Acta. 2016;1860(10):2211-9.
57. Li YW, Dudley AT. Noncanonical frizzled signaling regulates cell polarity of growth plate chondrocytes. Development. 2009;136(7):1083-92.
58. Rochard L, Monica SD, Ling IT, Kong Y, Roberson S, Harland R, et al. Roles of Wnt pathway genes wls, wnt9a, wnt5b, frzb and gpc4 in regulating convergent-extension during zebrafish palate morphogenesis. Development. 2016;143(14):2541-7.
59. Kamel G, Hoyos T, Rochard L, Dougherty M, Kong Y, Tse W, et al. Requirement for frzb and fzd7a in cranial neural crest convergence and extension mechanisms during zebrafish palate and jaw morphogenesis. Dev Biol. 2013;381(2):423-33.
60. Dougherty M, Kamel G, Grimaldi M, Gfrerer L, Shubinets V, Ethier R, et al. Distinct requirements for wnt9a and irf6 in extension and integration mechanisms during zebrafish palate morphogenesis. Development. 2013;140(1):76-81.
61. Gori F, Lerner U, Ohlsson C, Baron R. A new WNT on the bone: WNT16, cortical bone thickness, porosity and fractures. Bonekey Reports. 2015;4:6.
62. Kobayashi Y, Uehara S, Udagawa N, Takahashi N. Regulation of bone metabolism by Wnt signals. Journal of Biochemistry. 2016;159(4):387-92.

670 63. Ozeki N, Mogi M, Hase N, Hiyama T, Yamaguchi H, Kawai R, et al. Wnt16 Signaling Is
671 Required for IL-1 beta-Induced Matrix Metalloproteinase-13-Regulated Proliferation of Human Stem
672 Cell-Derived Osteoblastic Cells. International Journal of Molecular Sciences. 2016;17(2):14.
673 64. Kobayashi Y, Thirukonda GJ, Nakamura Y, Koide M, Yamashita T, Uehara S, et al. Wnt16
674 regulates osteoclast differentiation in conjunction with Wnt5a. Biochemical and Biophysical
675 Research Communications. 2015;463(4):1278-83.
676 65. Teh MT, Blaydon D, Ghali LR, Briggs V, Edmunds S, Pantazi E, et al. Role for WNT16B in
677 human epidermal keratinocyte proliferation and differentiation (vol 120, pg 330, 2007). Journal of
678 Cell Science. 2007;120(5):917-.
679 66. Dell'Accio F, De Bari C, Eltawil NA, Vanhummelen P, Pitzalis C. Identification of the molecular
680 response of articular cartilage to injury, by microarray screening. Arthritis and Rheumatism.
681 2008;58(5):1410-21.
682 67. Wergedal JE, Kesavan C, Brommage R, Das S, Mohan S. Role of WNT16 in the Regulation of
683 Periosteal Bone Formation in Female Mice. Endocrinology. 2015;156(3):1023-32.
684 68. Baker-LePain JC, Lane NE. Relationship between joint shape and the development of
685 osteoarthritis. Curr Opin Rheumatol. 2010;22(5):538-43.
686 69. Baker-Lepain JC, Lynch JA, Parimi N, McCulloch CE, Nevitt MC, Corr M, et al. Variant alleles of
687 the Wnt antagonist FRZB are determinants of hip shape and modify the relationship between hip
688 shape and osteoarthritis. Arthritis Rheum. 2012;64(5):1457-65.
689 70. Garcia-Ibarbia C, Perez-Nunez MI, Olmos JM, Valero C, Perez-Aguilar MD, Hernandez JL, et
690 al. Missense polymorphisms of the WNT16 gene are associated with bone mass, hip geometry and
691 fractures. Osteoporosis International. 2013;24(9):2449-54.

692